Int. J. Microgravity Sci. Appl., **34** (3) (2017) 340304
DOI: 10.15011//jasma.34.340304

IIIII AMS2016 Proceedings IIIII
(Original Paper)

Limiting Oxygen Concentration of Flame Resistant Material in Microgravity Environment

Keisuke MARUTA, Kandai TSUBOI and Shuhei TAKAHASHI

Abstract

Fire safety tests of materials used in the international space station have been conducted in normal gravity. However, in the previous researches, flame could spread in lower oxygen concentration in microgravity than in normal gravity. Therefore, it may cause fire hazard to use the ground-based flammability test results for microgravity environments. In the present paper, we modify our previous simplified model by including the effect of boundary layer on the material and compared the result with the parabolic flight experiment. Also we report the flammability limit of NOMEX, the typical flame resistant material obtained by parabolic flight experiments and compare it with PMMA. The results show that the minimum oxygen concentration (MLOC) of NOMEX was about 2% lower than that in normal gravity, and the flow velocity at MLOC is much larger (10~20cm/s) than that of PMMA (6~10cm/s). The feature of the flammability limit of NOMEX was successfully predicted by the modified model with the blow-off test data in forced flow.

Keyword(s): Flammability limit, NOMEX, Scale analysis, Microgravity
Received: 24 October 2016, Accepted 15 June 2017, Published 31 July 2017

1. Introduction

In recent years, human activity in space such as long-term missions in the International Space Station has increased. In closed environment such as the ISS, it is especially important to decrease fire hazards. On the other hand, extensive studies have reported that the flammability of solid materials readily expands in certain microgravity environments than under normal gravity conditions[1-6]. Sacksteder and Tien[7] have shown that the flammability limit, the limiting oxygen concentration vs. the opposed-flow velocity, is a U-shape curve, as **Fig. 1** shows. This figure implies that the flame spread can be enhanced in a mild opposed flow more than in natural convection.

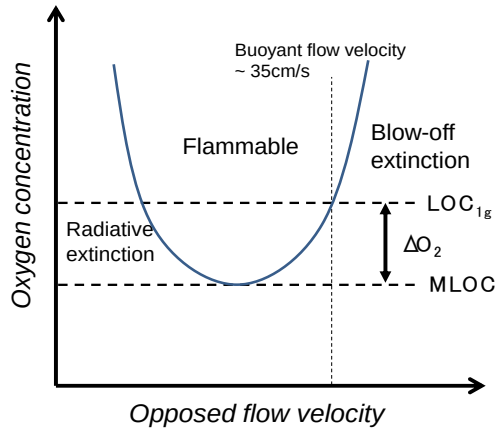

Fig. 1 Flammability map of a thin material with opposed flow.

In order to investigate the flammability of material in space, NASA STD-6001B[8] has been used, which is upward flame spread test. NASA STD-6001B is a pass/fail test; therefore, if the geometry of the material or the conditions under which the material is used changes, additional tests are required. This is inconvenient for choosing or developing new materials for space and new test estimating fire safety is desired. Hence, we focused on the ISO 4589-2 (LOI test). ISO 4589-2 is downward flame spread test and is good of reproducibility. Additionally, we have many ground-based flammability data because ISO 4589-2 have been conducted for several decades.

In the FLARE project, the International Space Station orbital experiment conducted by JAXA, one of the objectives is to develop a model for predicting the ΔO_2 from the LOI in ISO4589-2. The LOC_{1g} in **Fig. 1** is defined as the limiting oxygen concentration for downward spreading flame with a given sample geometry as mentioned later. Thus, the LOC_{1g} is not the same as LOI defined in ISO 4589-2. However, LOC_{1g} can be measured in normal gravity condition and it can work as an index as well as LOI. Hence, in the present paper, we introduce a method to predict the ΔO_2 from LOC_{1g} as the first step of the project. In our previous studies[9-11], we proposed a simplified model for predicting the effects of radiative loss and the finite kinetics on flame spread over a thermally thin material by scale analysis. In the present paper, we predict the flammability limit of PMMA film (ACRYPLEN, Mitsubishi Rayon), the base material, and NOMEX HT90-40, flame resistant material, and compare the predictions with flight

Gifu University, 1-1 Yanagido, Gifu-shi, Gifu 501-1193, Japan.
(E-mail: shuhei@gifu-u.ac.jp)

experimental results. Also, we discuss difference of features between NOMEX HT90-40 and PMMA.

2. Scale Analysis

In order to obtain expressions for the radiative heat loss and finite kinetic effects on flame spread rates over a thermally thin material, we set up heat balance for a two-dimensional flame, as shown in **Fig. 2**.

The length of the preheat zone, L_g, is assumed to be proportional to α_g/V_r. The virgin fuel receives heat via conduction driven by the temperature gradient in the gas-phase preheat zone. In the thermal regime, in which the opposed flow is moderate and both radiative losses and kinetic effects are negligibly small, the heat balance is expressed as

$$V_{f,th}\rho_s c_s L_{sy}(T_v - T_\infty) \sim \lambda_g \frac{(T_f - T_v)}{L_{gy}} L_{gx}$$

$$\text{, where } L_{sx} \sim L_{gx} \sim L_{gy} \sim \alpha_g / V_r \text{ and } L_{sy} = \tau \qquad (1)$$

$$\text{and } V_{f,th} \sim \frac{\lambda_g}{\rho_s c_s \tau} F \text{, where } F = \frac{T_f - T_v}{T_v - T_\infty}.$$

The obtained flame spread rate, $V_{f,th}$, is identical to the de Ris's expression[12]. When the opposed-flow velocity is very low, L_g becomes large and the radiative loss from the sample surface cannot be neglected (microgravity regime). Therefore, Eq. 1 can be rewritten as Eq. 2 in a microgravity regime, and it reduces to a simple nondimensional form by introducing a nondimensional spread rate, η (= $V_f/V_{f,th}$). Then

$$V_f \rho_s c_s L_{sy} W(T_v - T_\infty) + \varepsilon(1-\alpha_{abs})\sigma\left(T_v^4 - T_\infty^4\right) L_{gx} W$$
$$\sim \lambda_g \frac{(T_f - T_v)}{L_{gy}} L_{gx} W \qquad (2)$$

$$\eta + R_{rad} = 1 \text{, where } R_{rad} = B_2 \frac{\varepsilon(1-a_{abs})\sigma(T_v^4 - T_\infty^4)}{\rho_g c_g V_r (T_f - T_v)}$$

On the other hand, if the opposed-flow velocity is high, blow-off may occur due to the finite kinetic rate (kinetic regime). In such a situation, the Damkohler number, Da, is the important factor to consider when estimating the kinetic effect. Da is determined by the ratio of the characteristic residence time, t_{res}, to the characteristic chemical time, t_{chem}, but it can also be considered as the ratio of the total combustion heat of a pyrolysis gas in the preheat zone to the heat required to sustain a temperature gradient in the gas-phase preheat zone. Thus,

$$Da \equiv \frac{t_{res}}{t_{chem}} = \frac{L_g / V_r}{\rho_g / \dot{\omega}} = B_1 \frac{\alpha_g}{V_r^2} \rho_g Y_O A \exp(-E/RT_f)$$

or (3)

$$Da \equiv \frac{L_g / V_r}{\rho_g / \dot{\omega}} \sim \frac{{L_g}^2 \dot{\omega} \Delta h_c}{\rho_g c_g L_g V_r (T_f - T_v)} = \frac{{L_g}^2 \dot{\omega} \Delta h_c}{L_g \lambda_g (T_f - T_v)/L_g}$$

Hence, we made a model in which the heat conduction from the flame to the virgin fuel was reduced by the factor of (1−1/Da). Then, the heat-balance equation in the kinetic regime can be expressed as

$$V_f \rho_s c_s \tau W(T_v - T_\infty) \sim \left(1 - \frac{1}{Da}\right) \lambda_g \frac{(T_f - T_v)}{L_{gy}} L_{gx} W \qquad (4)$$

$$\text{or } \eta + 1/Da = 1$$

Coupling Eq. 2 with Eq. 4, we finally obtained the expression that holds through both the microgravity and kinetic regimes:

$$V_f \rho_s c_s L_{sy} W(T_v - T_\infty) + \varepsilon(1-\alpha_{abs})\sigma\left(T_v^4 - T_\infty^4\right) L_{gx} W$$
$$\sim \left(1 - \frac{1}{Da}\right) \lambda_g \frac{(T_f - T_v)}{L_{gy}} L_{gx} W \qquad (5)$$

$$\text{or } \eta + R_{rad} + \frac{1}{Da} = 1$$

Equation 5 implies that if the value of $R_{rad} + 1/Da$ is close to unity, the heat balance cannot be held and extinction occurs. In most cases, the relation $V_f << V_g$ holds, therefore $V_r = V_f + V_g$ can be replaced by V_g. In the above equations, we simply neglect the radiative heat transfer from the flame to the preheat zone because the flame near extinction is dim and both of the view factor and the emissivity of the gas-phase are sufficiently small.

The nondimensional parameters in both Eq. 2 and Eq. 4 are functions of the opposed-flow velocity, V_g, but it is thought that the effective flow velocities for the flame in the microgravity regime and the kinetic regime differ. In the microgravity regime, the opposed-flow velocity is very low and L_g becomes large. In this situation, the flow on the surface can be treated as a plug flow where the velocity profile is almost constant across the gas-phase preheat zone. On the other hand, in the kinetic regime, the L_g becomes small and the boundary layer on the surface has to be taken into account[13,14]. In order to simplify the model, we assumed a linear profile in the boundary layer[13] as shown in **Fig. 2**. With this assumption, the effective velocity is expressed as $V_{g,eff} \sim V_g L_g/\delta$, where δ is the boundary-layer

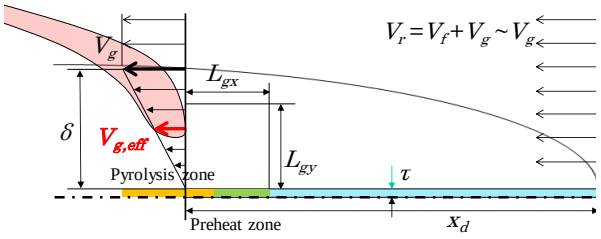

Fig. 2 Velocity profile in the vicinity of the flame front spread over a thin, flat material.

thickness. Some candidates for predicting the effective velocity seen by the flame front in the kinetic regime introduce the length Reynolds number, Re_x. In the present paper, we adopted a boundary-layer flow theory where the effective velocity is proportional to $Re_x^{-1/2}$, where Re_x is estimated using the length from the sample edge. By using the relations, $L_{gx} \sim \alpha_g / V_g$ and $\delta \sim x_d / Re_x^{1/2}$, we obtain

$$V_{g,eff} \sim \frac{V_g}{\mathrm{Pr}\,\mathrm{Re}_x^{1/2}} \tag{6}$$

In the present paper, we use the V_{eff} expressed by Eq. 6 for the kinetic regime, and therefore, the Damkohler number can be expressed as Eq. 7 instead of Eq. 3.

$$Da = B_1' \frac{\alpha_g}{V_g} \rho_g Y_O A \exp(-E / RT_f) \tag{7}$$

Using Eq. 5, Eq. 7 and the results of downward spread test as explained below, we calculate empirical activation energy, E and pre-exponential factor, A to predict the flammability limits for PMMA and NOMEX.

3. Experimental Apparatus

Figure 3 shows the experimental apparatus used for downward spread tests. The duct had a fan and the sample holder was set in the glovebox which is 1m x 1m x 1m (1000L); we could change oxygen concentration inside the glovebox. The dimension of the duct was 14 x 14x 35cm. The sample (PMMA, NOMEX), which was 8cm in length and 2cm in width was held by two thin (1mm thickness) stainless steel plates of C shape. The sample was set vertically in the center of the duct. The suction fan was set at the upper end of the duct to provide forced convection to the sample. Two honeycomb plates were set at the intake to rectify the flow. We varied the wind velocity in the duct by controlling the rotation of the fan.

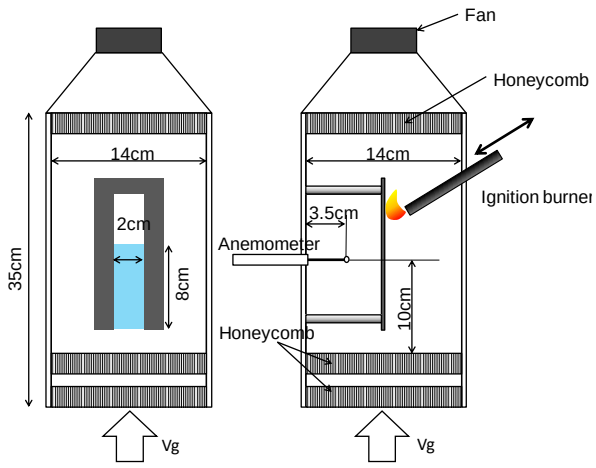

Fig. 3 Experimental apparatus for downward flame spread test.

In the experiment, we set the oxygen concentration in the glovebox at a desired concentration in advance, and then observed the flame spread with changing forced flow velocity. The wind velocity was measured by hot-wire anemometer which was set about 3cm apart from the sample. Ignition was conducted by inserting a burner through the hole on the duct wall and once the sample was ignited, the burner was removed. The hole for the ignition had a lid and after removing the burner, the lid closed not to disturb the flow in the duct.

The limiting oxygen concentration (LOC) was defined as the minimum oxygen concentration at a given forced flow velocity, in which the flame spread more than half of sample length, 4cm. If the sample was consumed more than 4cm, we defined the condition flammable, otherwise we defined it extinct. We changed the oxygen concentration and the forced flow velocity by 0.5% and 10cm/s, respectively. The blow-off tests in the buoyant flow and the forced flow were repeated 3 times for the same condition. Once the flame spread more than 4cm among the 3 tests, we defined the condition flammable. When we measure the LOC_{1g}, we also conducted downward flame spread test only with the natural convection, where we set the sample holder in the glovebox directly and the duct was not used. During the downward blow-off test, the change in the oxygen concentration in the glovebox was less than 0.1%.

We also conducted parabolic flight experiments to measure the flammability limits for PMMA and NOMEX in microgravity environments. The sample size was the same as in the downward spread tests. The details of the experimental apparatus are described in Refs. 11) and 16).

4 Results and discussions

Figure 4 shows the results of downward flame spread experiments. The horizontal axis is forced flow velocity and the vertical axis is the oxygen concentration. The circle symbol represents flammable condition and the cross represents extinct condition. The diamond represents the LOC_{1g}. The circle represents the minimum flammable oxygen concentration at a given forced flow, and the cross represents the condition in which the blow-off occurred in all 3 tests.

The limiting oxygen concentrations for PMMA and NOMEX increased with the forced flow velocity, respectively. This trend is consistent with Eq. 8 because the increase of oxygen concentration results in high flame temperature, T_f. **Figure 5** shows the calculated empirical activation energy, E and pre-exponential factor, A, assuming that the following two points lies on the blow-off limit; one is the blow-off condition with buoyant flow only, and the other is the blow-off condition with the forced flow in the horizontal axis. The buoyant flow is

assumed to be 35cm/s. For PMMA, the result shows that when the blow-off forced flow velocity is more than 70cm/s, the calculated E and A converged to a certain value and these were closed to the values in **Table 1**[15]. The emissivity of polymer material is typically 0.8~0.95 in mid-infrared region. In the present paper, we set the emissivity from the sample surface as unity for simplicity. On the other hand, if the forced flow velocity was close to buoyant flow velocity, the E and A are apart from those values. This discrepancy was caused by the coupling of buoyant flow and the forced flow; it was expected that the actual flow velocity seen by the flame was higher than that in pure forced flow condition when the forced flow velocity is small. This anticipation is consistent with the fact that the limiting oxygen concentration at Vg=40cm/s was 18.5 %, which is reasonably higher than its LOC_{1g}, which was 17%. Therefore, in the scale analysis, if we calculated empirical E and A from the blow-off experiment, we should adopt the result with high opposed flow velocity to neglect the effect of natural convection.

Figure 6 shows the results of flight experiments. The circle symbol shows flammable condition, and the cross shows the extinction. The triangle means the condition where flame spread for a while but went extinction in comparatively short time (about 10s) after ignition. The solid line in the **Fig. 6** is the limiting line which is derived by the scale analysis. The properties of PMMA in **Table 1** were used. The minimum limiting oxygen concentration (MLOC) of PMMA was 14.9 %

Table 1 Properties of PMMA for scale analysis[15]

	PMMA
Density, ρ_s (kg/m^3)	1190
Specific heat, c_s (kJ/Kg K)	1.465
Vaporization temperature, T_v (K)	670
Heat of combustion, Δhc (kJ/kg)	25900
Surface emissivity, ε	1.0
Pre-exponential factor, A (m^3/kg s)	1.36×10^9
Activation energy, E (J/mol)	1.50×10^5

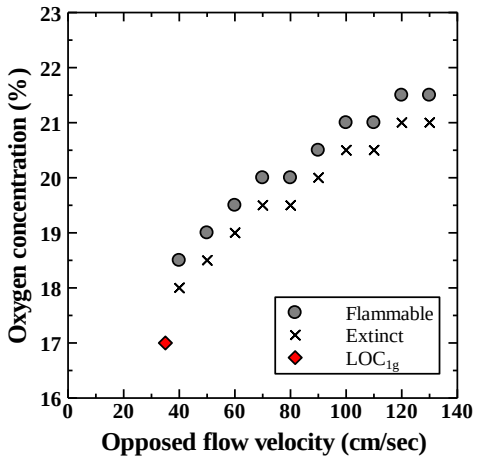

(a) PMMA

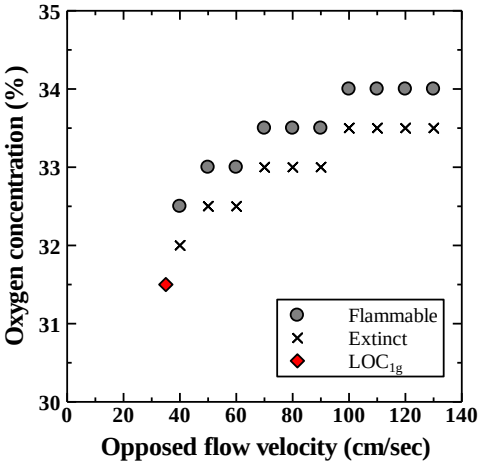

(b) NOMEX

Fig. 4 Limiting oxygen concentration of downward flame spread with forced flow.

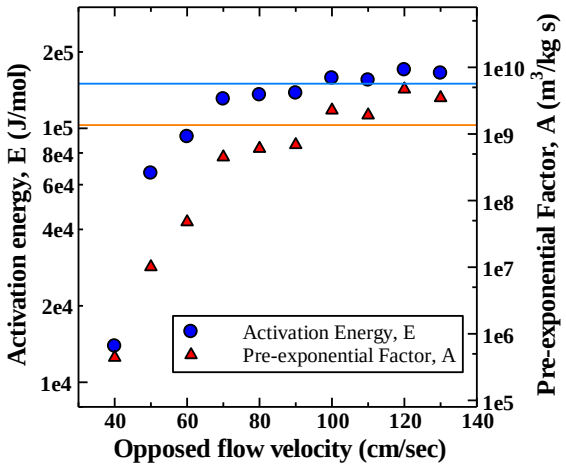

(a) PMMA

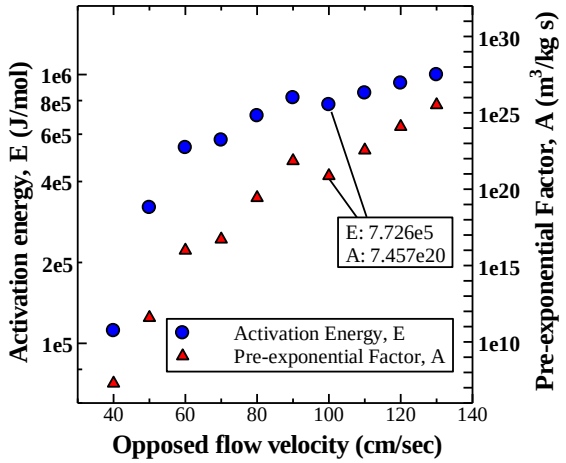

(b) NOMEX

Fig. 5 Empirical E and A calculated by downward flame spread experiments.

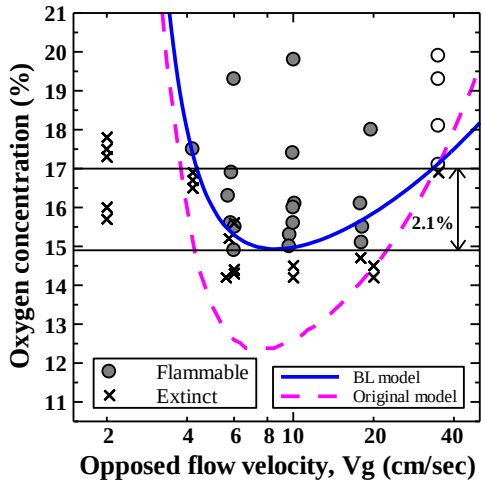

(a) PMMA

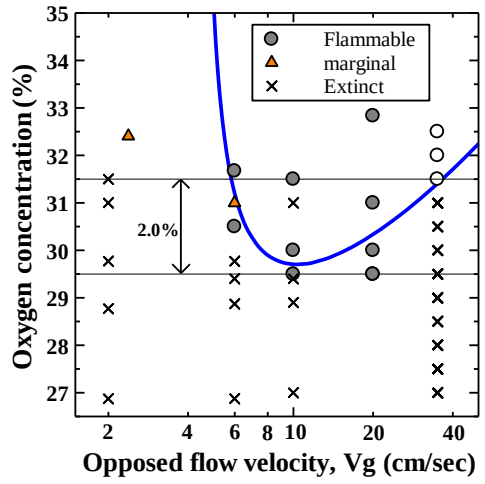

(b) NOMEX

Fig. 6 Flammability map obtained by flight experiment and the predicted limiting line by scale analysis.

when velocity was 6cm/s. The predicted limiting line well agrees with the results of parabolic flight experiment quantitatively. The dashed line shows the predicted limiting line of our previous work[11] with Eq. 3, in which the effect of the boundary layer is not taken into account. The previous prediction obviously overestimates the ΔO_2, which is the gap between MLOC and LOC_{1g}.

For NOMEX sheet, the MLOC was 29.5 % when the opposed flow velocity was 20cm/s. It is found that the MLOC of NOMEX is lower than the LOC_{1g}. It is also found that the velocity where the MLOC is observed is much higher than that of PMMA. The solid line shows the predicted limiting line by the scale analysis. In order to calculate the limit, the properties of NOMEX must be specified. However, such properties especially E and A are hardly available in literature. Hence, we first calculated empirical E and A as shown in **Fig. 5b**. Although there is some scattering due to the coarse interval of tested oxygen concentration (0.5%), the calculated activation energy for NOMEX shows almost flat distribution between 80cm/s and 110cm/s. Hence, The limiting oxygen concentrations with natural convection (LOC_{1g}) and with the forced flow of 100cm/s were used as the representative value. According to **Fig. 5b**, E was 7.726e5 and A was 7.457e20. Additionally, we assumed that the pyrolysis temperature of NOMEX was 750K[17], which is 80K higher than that of PMMA.

The predicted limiting line agrees with the trend of the flammability of NOMEX. The higher pyrolysis temperature moves the radiative extinction limit toward high opposed velocity side due to larger radiative heat loss from the preheat zone to the surroundings. This means that the NOMEX does not burn in low opposed flow conditions and this trend was consistent with the experimental results. The calculated MLOC was 29.7%, which was close to the actual MLOC, 29.5%. It is found that the empirical E and A can yield reasonable prediction in spite of the simplicity of the model.

In the modified model, we included the effect of boundary layer to introduce the effective flow velocity relative to the flame front. With this modification, we could consider the effect of bulk flow velocity on blow-off phenomena correctly. Additionally, the blow-off tests provided proper empirical values for Eq. 8, which represents the actual blow-off blanch of the material. Although the MLOC is calculated with the radiative effect and the kinetic effect, the accuracy of the blow-off blanch has more effects on the MLOC because these kinetic parameters generally contain larger uncertainty. Therefore, it is important to predict the blow-off blanch precisely. In other word, the proposed method extrapolates the blow-off blanch toward mild or low flow velocity region correctly with blow-off test data at high flow region to predict reasonable MLOC.

5 Conclusions

In order to predict the MLOC of thin, flat materials in microgravity environments, we developed a simplified model for the flame spread over a material with an opposed flow. In the present paper, we showed the results of scale analysis including boundary layer theory in the kinetic regime. By using the results of ground-based flame spread data, we could show more quantitative prediction for PMMA sheet by scale analysis. We also compared the result of flight experiment of PMMA with that of NOMEX. We found that flow velocity of NOMEX with MLOC was higher than that of PMMA. This trend resulted from the fact that the vaporization temperature of NOMEX was higher and the radiative energy loss from preheat zone was large. We also attempted to calculate the limiting line for NOMEX sheet by using the result of blow-off tests. The prediction well agreed with the result of the parabolic flights, which implied the validity of the developed simplified model.

Nomenclatures

A	Pre-exponential factor
a_{abs}	Absorption coefficient of gas, $a_{abs} = 0$
B_1	Empirical constant for Da
B_2	Empirical constant for R_{rad}, $B_2 = 2.67$
c_g	Specific heat of gas
c_s	Specific heat of solid
Da	Damkohler number
E	Activation energy
Δh_c	Heat of combustion
L_{gx}	Gas-phase diffusion length in x-direction
L_{gy}	Gas-phase diffusion length in y-direction
L_{sx}	Solid-phase diffusion length in x-direction
L_{sy}	Solid-phase diffusion length in y-direction, $L_{sy}=\tau$
R_{rad}	Radiation loss factor
T_f	Adiabatic flame temperature
T_v	Pyrolysis temperature
T_∞	Ambient temperature
t_{chem}	Characteristic chemical time
t_{res}	Characteristic residence time
V_g	Opposed flow velocity
$V_{g,eff}$	Effective flow velocity seen by the flame front
V_f	Flame spread rate
$V_{f,th}$	Flame spread rate in thermal regime
V_r	Velocity relative to flame, $V_r = V_g + V_f \sim V_g$
W	Sample width
x_d	Distance from the sample edge
α_g	Thermal diffusivity of gas, evaluated at T_v
ε	Surface emissivity, $\varepsilon = 1$
λ_g	Gas-phase conductivity evaluated at T_v
λ_s	Solid-phase conductivity
η	Non-dimensional spread rate, $\eta = V_f / V_{f,th}$
ρ_g	Gas density evaluated at T_v
ρ_s	Solid density
τ	Fuel half-thickness
ω	Gas-phase reaction rate

References

1) H. Shih and J. S. Tien: Proc. Combust. Inst., **28** (2000) 2777.
2) K. Prasad, Y. Nakamura, S. L. Olson, O. Fujita, K. Nishizawa, K. Ito and T. Kashiwagi: Proc. Combust. Inst., **29** (2002) 2553.
3) T. Kashiwagi, K.B. McGrattan, S.L. Olson, O. Fujita, M. Kikuchi and K. Ito: Proc. Combust. Inst., **26** (1996) 1345.
4) S.L. Olson, P.V. Ferkul and J.S. T'ien: Proc. Combust. Inst., **22** (1989) 1213.
5) S.L. Olson and F.J. Miller: Proc. Combust. Inst., **32** (2009) 2445.
6) S.L. Olson, T. Kashiwagi, O. Fujita, M. Kikuchi and K. Ito: Combustion and Flame, **125** (2001) 852.
7) K.R. Sacksteder and J.S. Tien: Proc. Combust. Inst., **25** (1994) 1685.
8) NASA-STD-6001 B: Flammability, Offgassing, and Compatibility Requirements and Test Procedures (2011).
9) S. Bhattacharjee, J. West and R.A. Altenkirch: Proc. Combust. Inst., **26** (1996) 1477.
10) S. Bhattacharjee, S. Takahashi, K. Wakai and C. Paolini: Proc. Combust. Inst., **33** (2011) 2465.
11) S. Takahashi, T. Ebisawa, S. Bhattacharjee and T. Ihara: Proc. Combust. Inst., **35** (2015) 2535.
12) J.N. de Ris: Proc. Combust. Inst., **12** (1969) 241.
13) I.S. Wichman: Combustion and Flame, **50** (1983) 287.
14) S. Bhattacharjee, W. Tran, M. Laue, C. Paolini and Y. Nakamura: Proc. Combust. Inst., **35** (2015) 2631.
15) A.C. Fernandez-Pello, S.R. Ray and I. Glassman: Proc. Combust. Inst., **18** (1981) 579.
16) K. Tsuboi, K. Maruta, S. Takahashi, T. Ihara and S. Bhattacharjee: Trans. JSASS Aerospace Tech. Japan, **14** (2016) Ph_1.
17) S. Villar-Rodil, A. Martinez-Alonso and J.M.D. Tascon, J. of Analytical and Applied Pyrolysis, **58-59** (2001) 105-115.